Cloud 3D effects on broadband heating rate profiles: I. Model simulation

Lei Song [a,b], Qilong Min [a,*]

[a] Atmospheric Sciences Research Center, State University of New York, Albany, NY 12203, USA
[b] Key Laboratory of Middle Atmosphere and Global Environment Observation, Institute of Atmospheric Physics, Chinese Academy of Sciences, Beijing 100029, China

ARTICLE INFO

ABSTRACT

Solar broadband heating directly drives the atmospheric and ocean circulations, and is largely determined by cloud spatial 3-diminesional (3D) structures. To study the cloud 3D effects on radiation, a 3D broadband Monte-Carlo radiative transfer model, along with an Independent Pixel/Column Approximation (IPA) method, is used to simulate radiation and heating rate of three typical cloud fields generated by cloud resolving models (CRM). A quantitative and statistical estimation of cloud 3D effects has been developed to investigate the impact of cloud 3D structures on both heating rate strength, *STD_Bias*, and vertical distribution, *CorrCoef*. The cloud 3D structures affect some clouds more in heating rate strength and others more in vertical distribution. It is crucial to use the combination of *CorrCoef* and *STD_Bias* for better quantitative evaluation of the 3D effects. Furthermore, there is no simple way to define a critical resolution (or average radius), within which the IPA heating rate profiles closely represent the true 3D heating rate profiles. The critical radius (or resolution) strongly depends on solar incident angle as well as cloud vertical distribution. Also, the critical radii for clear-sky columns are larger than for cloudy columns, although the corresponding *STD_Bias* for clear-sky columns are smaller than for cloudy columns. Analysis based on two different statistical average methods illustrates that the cloud 3D effects due to the dimensionality difference between the 3D clouds (circle average) and 2D clouds (line average) significantly impact on the heating rate profiles.

© 2010 Elsevier Ltd. All rights reserved.

1. Introduction

Clouds play a critical role in the balance of the atmospheric energy budget and hence in earth's climate system [1–4]. The climate system converts solar radiation into heat and the heating directly drives the atmospheric and ocean circulations. The incomplete knowledge of clouds, radiative forcing, and cloud feedback limits our understanding of detailed mechanisms of climate change [5]. It is well known that the distributions of heating rate profiles strongly depend upon the cloud three-dimensional (3D) vertical structures [6–8]. Therefore, to understand the effects of cloud 3D structures on broadband heating rate profiles is crucial to understand cloud feedback in the climate system.

Since General Circulation Models (GCM) treat cloud–radiation interaction with Plane-Parallel and Homogeneous (PPH) assumption, the impact of cloud 3D distributions on radiative transfer calculation is neglected in the large scale grids. Several studies demonstrated the bias of this simple PPH assumption to the real 3D situation [9–12]. The Independent Pixel/Column Approximation (IPA/ICA) method is considered to be a better approach than PPH in predicting the domain average

---

* Corresponding author.
E-mail address: min@asrc.cestm.albany.edu (Q. Min).

radiative properties [13–16]. However, the IPA method neglects radiation horizontal transport, which results in remarkable bias when clouds have complicated structures [14,17–22].

Many efforts of investigating 3D cloud effects are focused mainly on the large scale or domain average results [10,22–29]. For example, Barker et al. [10,23] showed that the domain averaged heating rate profiles depend fairly weakly on cloud geometry. However, Hinkelman et al. [22] argued that cumulus cloud geometry can cause changes of 10–17% in domain average heating rate profiles. Fu et al. [29] pointed out that for a cluster of deep convective cloud systems, the average daytime absorption derived from full 3D simulation is more than 20 W m^{-2} larger than the IPA estimate.

As GCMs and Cloud Resolving Models (CRM) are improved in spatial resolution, it is necessary to assess the cloud 3D effects under high resolution conditions [30–33]. O'Hirok and Gautier [34] demonstrated that 2–5 km is a critical resolution for cloud 3D effects. When a model resolution is larger than this threshold for their selected cases, the IPA approach is accurate enough. Di Giuseppe and Tompkins [35] also found that the geometry-related effects can have a larger influence on radiative transfer calculations than internal optical inhomogeneity for the CRM resolved tropical deep convective clouds.

Most of those studies are focused on the surface or the top of the atmosphere (TOA) radiation fluxes. However, the radiation closure at the boundaries cannot ensure the accuracy of the heating profile [36]. The erroneous heating rate distribution due to the simplification of RT calculation would impact on cloud formation and dynamics. Also cloud 3D effects are an important issue for remote sensing. Hence, with improving model and measurement spatial resolutions, more attention should be paid to the cloud 3D effects on the vertical distribution of heating rate. As the first of our series researches, this work will focus on a quantitative assessment of the cloud 3D effects on heating rate profiles, particularly from both modeling and observational perspectives. With the basic understanding and evaluation of the 3D effects on heating rate profiles, we will seek ways to detect the 3D effects in addition to current imaging instruments or vertical resolved active sensors in the follow-on research.

2. Cloud fields and radiative transfer model

2.1. CRM cloud fields

Three CRM-resolved cloud fields, named as ATEX, Open-cells, and GATE-A, are selected from the InterComparison of Radiation Codes in Climate Models (ICRCCM) program phase III and used in our radiation simulation. Fig. 1 illustrates their main optical properties. They are typical cloud fields with different cloud patterns, domain areas, and resolutions, enabling a comprehensive study of the impact of cloud 3D effects on heating rate profiles. Although some clouds are mixed phase clouds, they are all treated as water droplets with effective radius of 10 μm to simplify the calculation. These simplifications are the same as done in ICRCCM [37].

ATEX (Fig. 1a) is generated for the Atlantic Trade Wind Experiment (ATEX) [37]. It is a marine boundary layer cloud which extends from about 0.7 to 1.6 km. The horizontal resolution is 0.1 km and the domain size is (6.8 km)^2. The vertical resolution varies from 0.02 to 0.04 km in the cloudy parts. Most clouds locate around 1.5 km and the average extinction coefficient β is about 100 km^{-1}. The cloud fraction A_c decreases at lower layers while β increases to about 200 km^{-1}.

GATE-A (Fig. 1b) is extracted from the simulation of phase III of the Global Atmospheric Research Program—Atlantic Tropical Experiment (GATE) [38]. This cloud consists of non-squall clusters of organized convection with the anvil removed so as to mimic towering or developing clouds. The deep convective clouds extend up to to 8 km in this field. The horizontal resolution is 2 km and the domain size is (400 km)^2. The vertical resolution varies from 0.2 km to several km. The typical β is about 60 km^{-1}. Both geometric and optical depths are thick in this cloud field.

The Open-cells (Fig. 1c) represent a cold-air outbreak over warm water, consisting of strong open cellular convection clouds [39]. Vertical and horizontal resolutions are 0.15 and 0.39 km, respectively. The entire cloud field is about (50 km)^2. The main layer locates between 4 and 7 km, with a lower thick cloud layer at about 2 km. The extinction coefficient β is about 30 km^{-1} for the upper-layer clouds, and about 70 km^{-1} for the low-level clouds.

2.2. Radiative transfer model

We use a broadband 3D Monte-Carlo radiative transfer model to calculate broadband SW radiation. The spectral range is from 50,000 to 2500 cm^{-1}. Non-gray gaseous absorptions, including H_2O, CO_2, O_3, CH_4, and N_2O, are parameterized based on the correlated κ-distribution method, with 54 bins in 6 SW bands [40]. The other details of the model are described by Barker et al. [10]. The IPA calculations use the same 3D model by setting the horizontal resolution as infinite in each column, ignoring the horizontal transport between the columns. Both true 3D Monte-Carlo simulation and IPA calculation will simply be referenced by 3D and IPA.

All three cloud fields are simulated at 10 solar zenith angles (SZA) with an interval of cosine (SZA) of 0.1 for domain average calculation and validation, and at 4 SZAs of 0°, 30°, 45°, and 60° for detailed heating rate calculation. Both 3D and IPA approaches are calculated for comparison. The solar azimuth angle is 0°. The surface albedo is set to be a constant of 0.2. Sufficient photons are emitted to ensure the convergence for the Monte-Carlo simulation.

Before detailed analysis, our 3D results are validated against the benchmark of the ICRCCM, which is the average result from several 3D models [37]. Fig. 2a and b shows the domain average transmittances with different SZAs and the domain average heating rate profiles at SZA of 60° SZA for all three cloud fields, respectively.
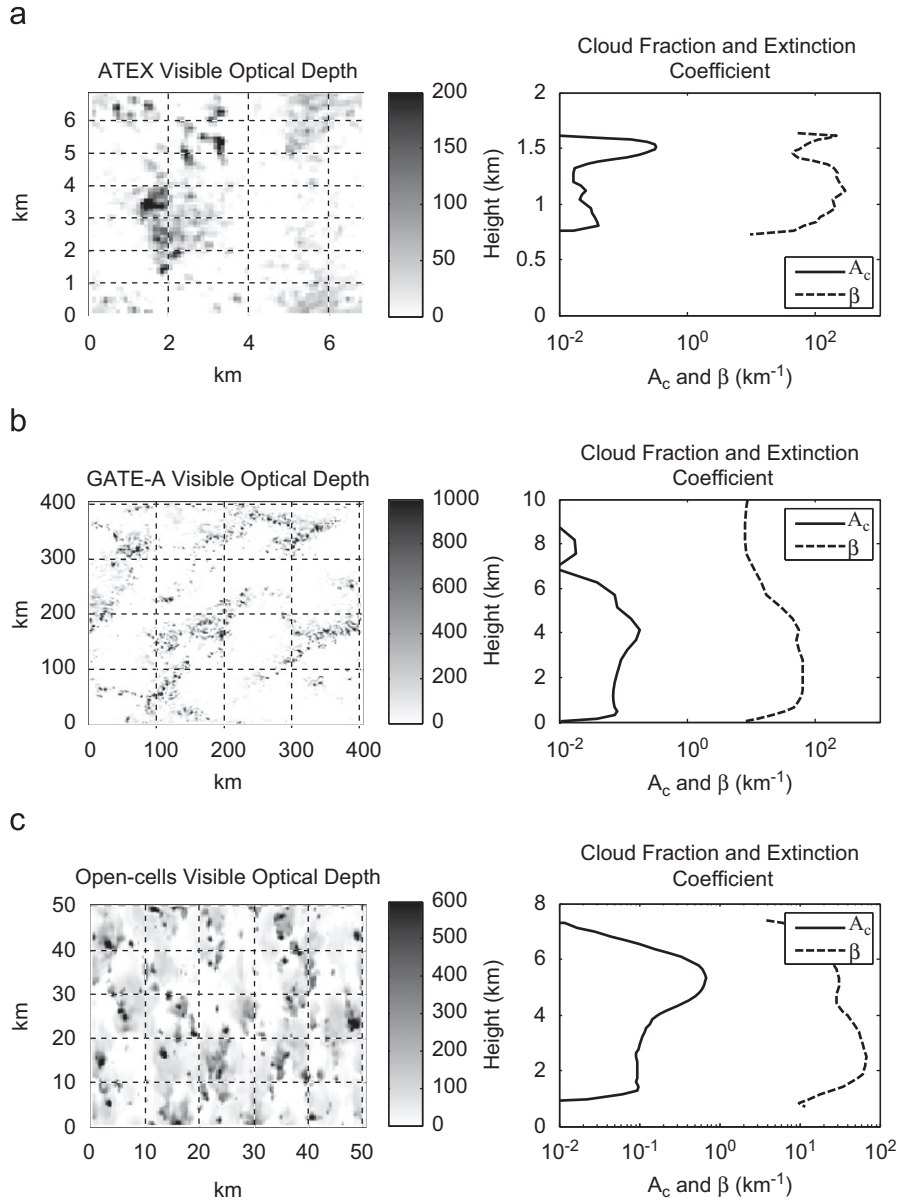
Fig. 1. The optical properties of three cloud fields, including vertical integrated visible optical depth, cloud fraction A_c and extinction coefficient β, respectively.

The validation shows a good agreement between our results and the benchmark.

3. Statistical parameters and methods

3.1. Statistical parameters

To evaluate the vertical distribution of heating rate, two parameters, *CorrCoef* and *STD_Bias*, are used to quantify the similarities and differences between each pair of heating rate profiles. They are very similar to the traditional definitions of correlation coefficient and standard deviation, with some modifications for the current application.

For a given pair of profiles, vectors $HR_{3D}(n)$ and $HR_{IPA}(n)$ where n is from 1 to N and N is the layer of the profile, we calculate the covariance matrix *Cov* by

$$Cov(HR_{3D}, HR_{IPA}) = E[(HR_{3D} - \mu_{3D})(HR_{IPA} - \mu_{IPA})] \qquad (1)$$

where E is the mathematical expectation and $\mu_i = EHR_i$. The *CorrCoef* is calculated by

$$CorrCoef = \frac{Cov(HR_{3D}, HR_{IPA})}{\sqrt{\sigma_{3D}\sigma_{IPA}}} \qquad (2)$$

where σ_i is the variance and $\sigma_i = E(HR_i - E(HR_i))^2$. The *CorrCoef* quantifies the similarity of the two vertical profiles.
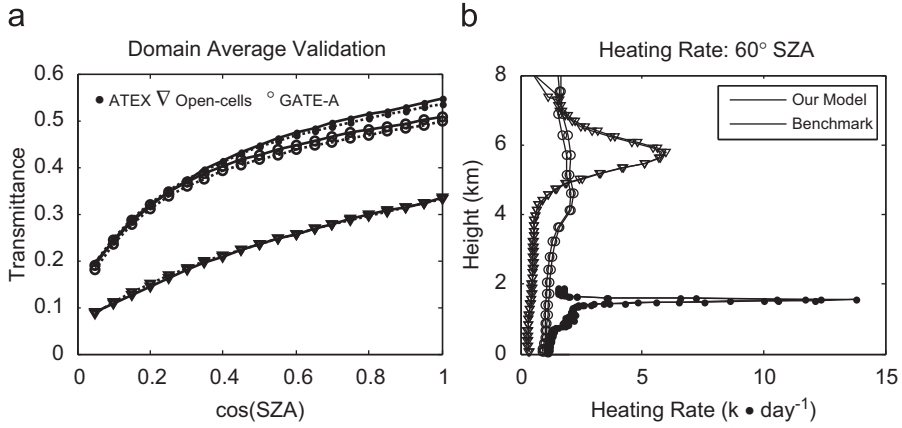
Fig. 2. (a) Validation of domain average transmittances changing with SZA between our results and the ICRCCM benchmark of three cloud fields. (b) Similar validation of average heating rate profiles at 60° SZA. The solid lines are our results and the dashed lines are the benchmarks. Different cloud fields are marked by different symbols.
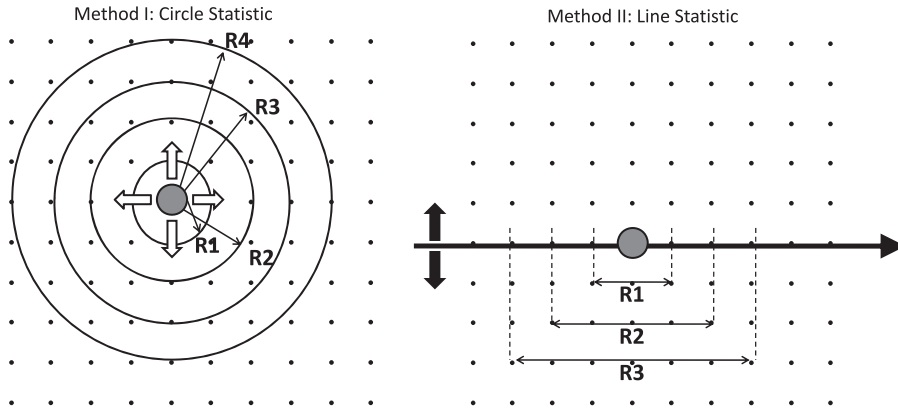

Fig. 3. Schematic of two statistical methods. Left panel shows Method I and right panel shows Method II.

To define the difference between the two vertical profiles, we first calculate the parameter STD defined as

$$STD = \sqrt{\frac{\sum_{i=1}^{n}(HR_{3D}(i) - HR_{IPA}(i))^2}{n}} \qquad (3)$$

Then the STD_Bias is defined as

$$STD\_Bias = \left(\frac{STD}{\overline{HR_{3D}}}\right)100 \qquad (4)$$

where $\overline{HR_{3D}}$ is the mean of the relative 3D heating rate. The STD_Bias is the percentage of the bias to the mean value of the 3D heating rate. Considering the heating rates of three cloud fields are compared together, the STD_Bias is better than the STD to quantify the relative difference between the two vertical profiles. Combination of these two parameters not only describes the deviation of the heating rate strength, but also directly represents the vertical properties of the heating rate.

3.2. Statistical methods

Two statistical methods are applied to show the cloud 3D effects on the heating rate profiles: Method I (Circle statistics) and Method II (Line statistics). The schematic of Method I is shown as the left panel in Fig. 3. For each column, the average radius changes from 1 column to 20 columns to get 20 circle areas for different resolutions. In each circle area, two average heating rate profiles over the area are calculated by both 3D and IPA approaches. And then the CorrCoef and STD_Bias between these two profiles are obtained. For each radius (or resolution), the statistical mean CorrCoef and STD_Bias of all columns within the simulation domain are calculated. Note that the spatial resolution is twice the corresponding radius. This scenario represents a statistical average in most applications in numerical models and satellite imager/scanning measurements.

Many observations, fixed-view sensors at both surface and satellite, cannot obtain all the data in a domain area. To mimic this kind of observation, we use Method II (Line statistic). The radius still changes from 1 column to 20 columns for each column, but only columns along a line through this central one will be included in our statistical analysis. We set the line's azimuth to be the same as the solar incidence angle (0°). The schematic of Method II (Line statistic) is shown as right panel in Fig. 3. The rest of the statistical processes are the same as Method I.

4. Results

4.1. Domain average results

Before proceeding into detailed analyses, we first studied the domain average results. Fig. 4 shows the comparison of domain averaged transmittance, reflectance, and absorptance between the 3D and the IPA. In general, the IPA results reasonably agree with the 3D results. The IPA tends to be more transmissive (less reflective) at low SZAs, and less transmissive (more reflective) at larger SZAs than the 3D, regardless of the cloud fields, as the IPA neglects the cloud side leakage for overhead sun and the cloud side illumination for low sun. Furthermore, the IPA column absorption is always less than the 3D with the maximum bias at an intermediate SZA. Such bias patterns can be explained by the lack of horizontal transport in the IPA approach. The horizontal fluxes always increase photon path length, resulting in an increase of column absorption for the 3D. Clearly, the bias in the Open-cells case is relatively larger than the other cases. As the Open-cell cloud field has more broken structures, more photons are trapped between cloudy pixels, thus accumulating water vapor absorption.

The bias in the heating rate profile varies with SZA and is more obvious at high SZA value, shown in Fig. 5. Vertically, the largest heating rate bias in current simulations occurs within the clouds where cloud fraction is maximum in the profiles as shown in Fig. 1. At the lower altitude under this part, the bias is increasing when the sun is more oblique, as more photons penetrate into clouds and are scattered into horizontal transport that enhances the atmospheric absorption.

4.2. Heating rate profile with different statistical methods

Different average radius and/or methods would result in different heating rate profiles, particularly for high resolution applications. Fig. 6 shows an example, a subset of the Open-cells cloud field, to illustrate the cloud 3D effects for various methods with different radius. Simulation is done for SZA at 45°. The central column, the column (37, 52) in the Open-cells domain, is a multi-layer cloud (Fig. 6b), with some multi-layer clouds and some single high-level clouds around it (Fig. 6a). The mean heating rate profiles at different average radius for Methods I and II are shown in Fig. 6c and d, respectively. The results of Method I indicate that, for small radius (e.g. $R=2$), the lack of horizontal transport in the IPA results in the overestimation of heating rate at the upper-layer cloud and underestimation at the lower-layer cloud, with respect to the 3D heating rate profile and much worse to the central column heating rate profile. As clouds
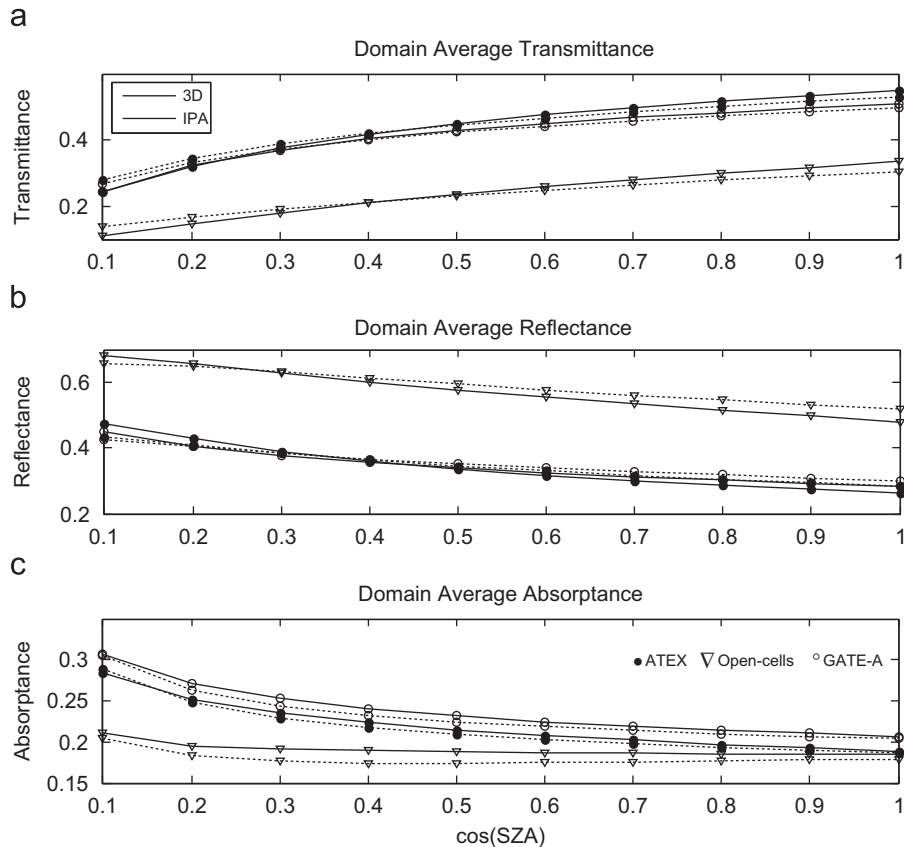

Fig. 4. Domain average transmittance (a), reflectance (b), and absorptance (c) of three cloud fields at different SZAs. The solid and dashed lines represent the 3D and the IPA, respectively. Different cloud fields are marked by different symbols.
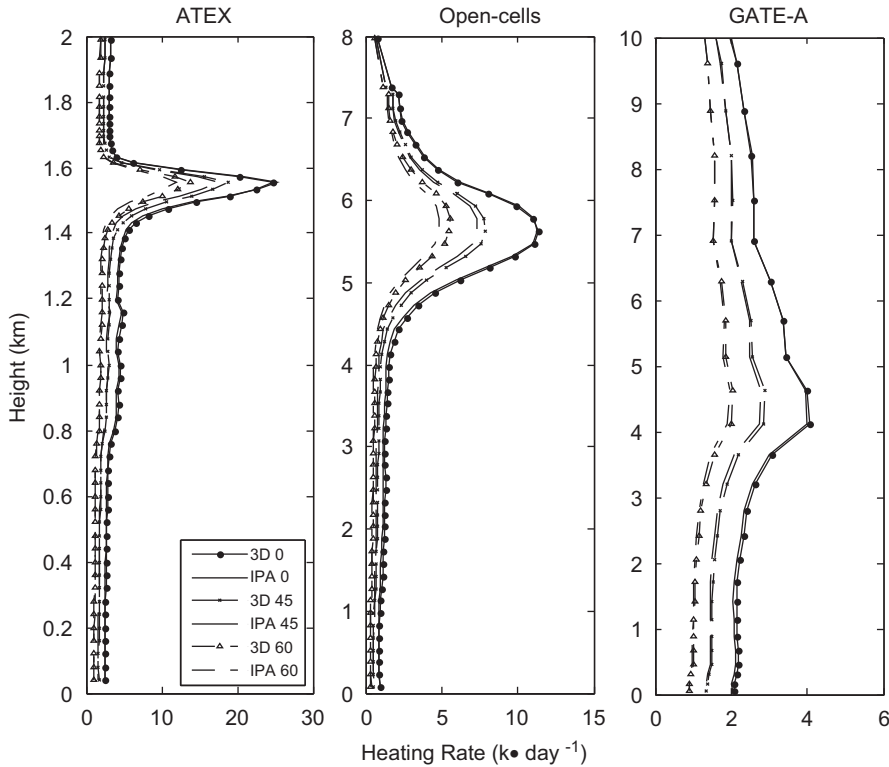
Fig. 5. Domain average heating rate profiles of three cloud fields. SZA is represented by different line type. The Lines with and without symbols mean the results of the 3D and the IPA, respectively.

clustered with many upper-level clouds, the vertical distribution of average profiles converges to the upper layer in a short range. On the other hand, the heating of lower layer disappears for large average radii, as more single high-level clouds occurred in the ranges. The lack of heating of lower layer compared to the 3D results would certainly change the evolution of the low-level clouds, and consequently the entire cloud system. In general, it is clear that the vertical distributions of heating rate of the IPA are getting closer to those of the 3D with increasing average radius in both methods. In Method II, due to the limit of samples and the dimensionality difference, there is a substantial difference between the Methods I and II, in both the 3D and the IPA.

To illustrate the cloud 3D effects on inhomogeneous distribution of heating rate, we mimic the observation along the satellite track or time series of a surface observation. Fig. 7 is a slice view for the Open-cells case with SZA of 45°. All results are calculated by Method II. In a range of 40 km, the cloud field is composed by clear-sky, thick convective clouds, and thin clouds (Fig. 7a). Comparing the 3D and IPA results in Fig. 7b and c, there is an obvious illuminating-effect towards the incident direction and shadowing-effect at the opposite direction at the top layers. Furthermore, the 3D results show an upward shift, which is consistent with the previous findings [34,35]. This 'erroneous heating' is further examined at different resolutions, shown in Fig. 7d and e. At a resolution of about 4 km (5 columns in radius), the

average process does not significantly improve the heating rate profiles, i.e., the heating rate is still obviously underestimated in cloudy columns and overestimated in clear columns. At a resolution of about 10 km (12 columns in radius), one column may contain both clear-sky and cloudy atmosphere. At such a large average domain, the differences between the 3D and the IPA are substantially reduced. However, there is still some bias in vertical distribution, particularly in a column with thin and broken clouds from 24 to 34 km where the differences are still in a range from −2 to +2 k/day.

For high spatial resolution applications in either modeling or remote sensing, to ignore the cloud 3D effects and to directly use the averaged results of a large area would lead to substantial errors in local heating rate profiles. The solar radiation may heat some columns a few kilometers away from the correct ones. The shift of erroneous heating at lower layers is largely determined by solar incident angle and associated with photon horizontal transport. The tilted IPA (TIPA) [21,22] may be sufficient to deal with the shift associated with solar incident angle by calculating the photon transport in independent columns towards the direction of incident radiation. However, the lack of photons horizontal transport in the IPA or TIPA may still result in certain errors in the heating rate profile, even with a resolution of 10 km. The wrongfully heated columns certainly would affect the accuracy of model simulations and retrievals.
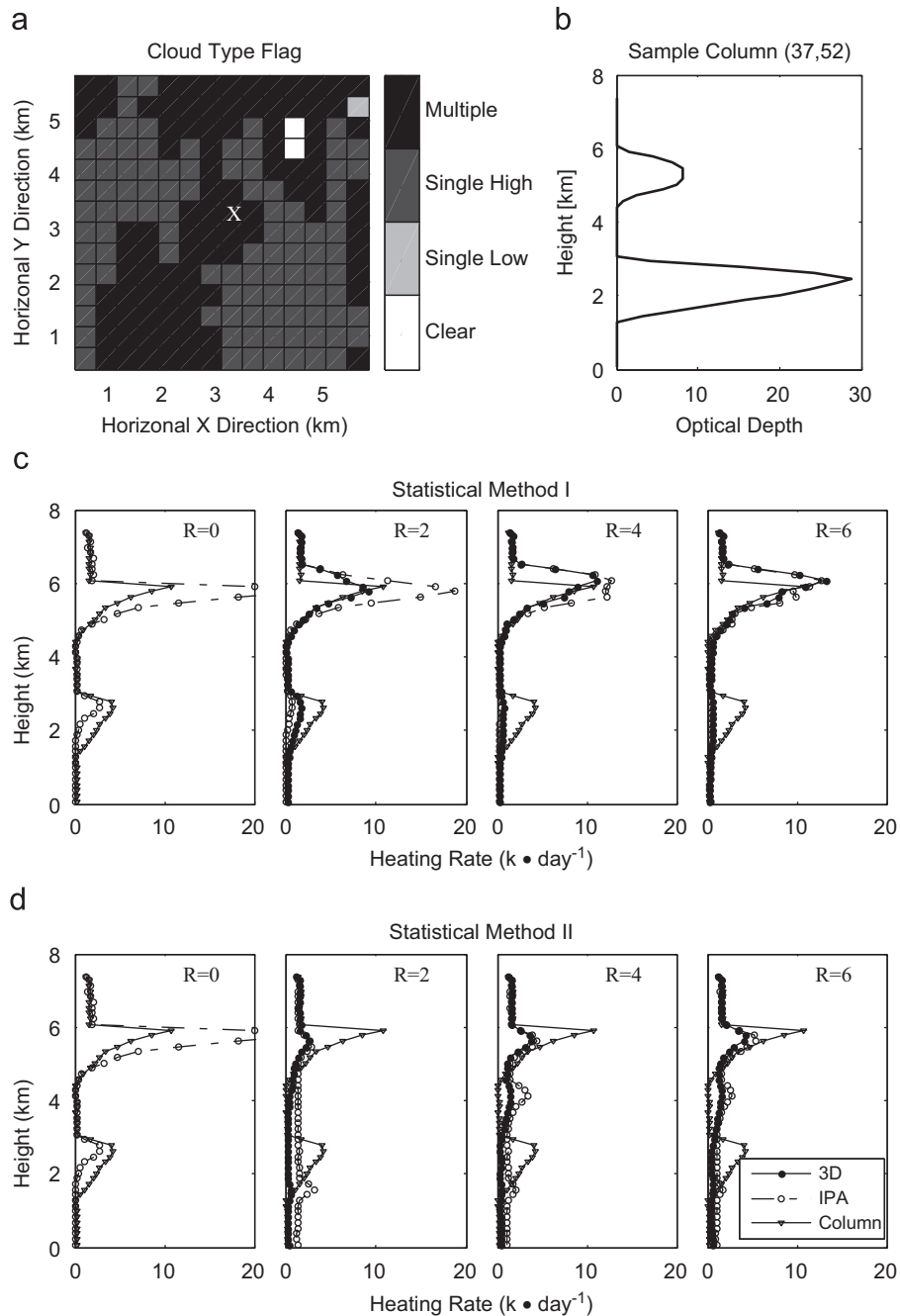
Fig. 6. A sample of smooth process in Open-cells at 45° SZA. (a) Cloud types around the central column (marked by symbol X), (b) the vertical distribution of cloud visible optical depth of the central column, (c) the averaged heating rate profiles for both the 3D and the IPA with different radii by Method I, and (d) the same as (c) but by Method II.

4.3. Statistical analysis

To quantitatively illustrate the cloud 3D effects, the statistical results are evaluated for all three cloud fields with various SZAs and the two average methods. Fig. 8 shows the mean *CorrCoef* and *STD_Bias* for Open-cells and GATE-A as a function of average radius. In general, the *CorrCoef* increases and the *STD_Bias* decreases with average radius. At the scale of about 5 km in radius in Open-cells (and 10 km in radius in GATE-A), the improvements in both *CorrCoef* and *STD_Bias* start to diminish, indicating the IPA bias in the heating rate profile cannot be completely eliminated. At such a scale, the photon horizontal transport dominates the bias. Also, the *CorrCoef* decreases and the *STD_Bias* increases with SZA, especially with small average radius. The difference
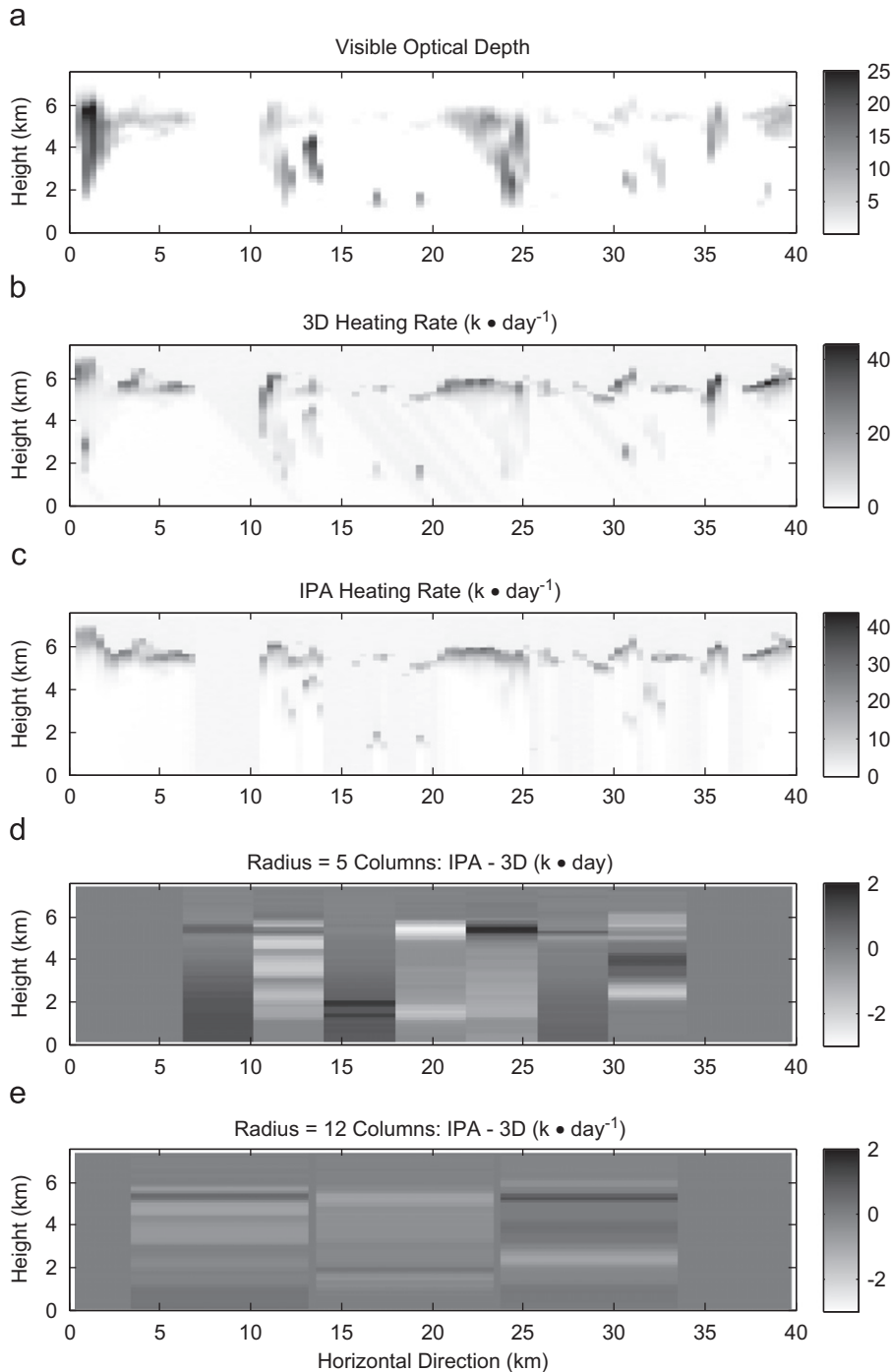
Fig. 7. A sample of slice view in Open-cells at 45° SZA. (a) The cloud visible optical depth distributions, (b) and (c) the heating rate distributions of the 3D and the IPA, respectively, and (d) and (e) the differences of heating rate distributions between the IPA and the 3D calculated by Method II for the resolution of 4 and 10 km, respectively.

associated with SZA is reduced significantly with the average radius. However, the difference between Methods I and II increases with the average radius, due to the fundamental difference in dimensionality between the 3D clouds and the 2D clouds, and to a lesser extent, insufficient samples. It has serious consequences, as

many derived heating rate profiles from observations with fixed view sensors, such as broadband heating rate profile (BBHRP) products from current atmospheric radiation measurement (ARM) facilities.

Our three cloud fields have distinct cloud structures as well as different domain and column resolutions.
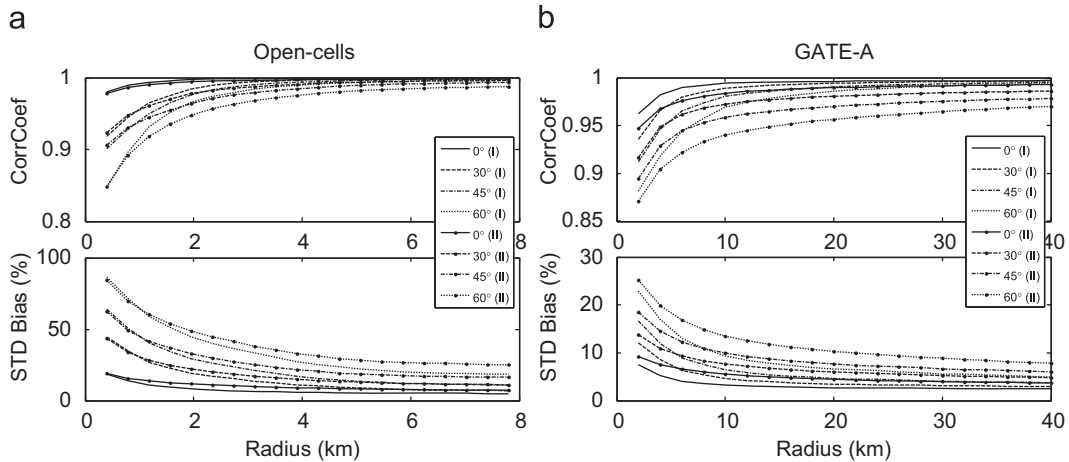
Fig. 8. The average *CorrCoef* and corresponding *STD_Bias* of Open-cells (left two panels) and GATE-A (right two panels) calculated by both methods at different SZAs changing with the statistic radius. SZA is represented by different line types. The Lines without and with symbols mean the results of Methods I and II, respectively.
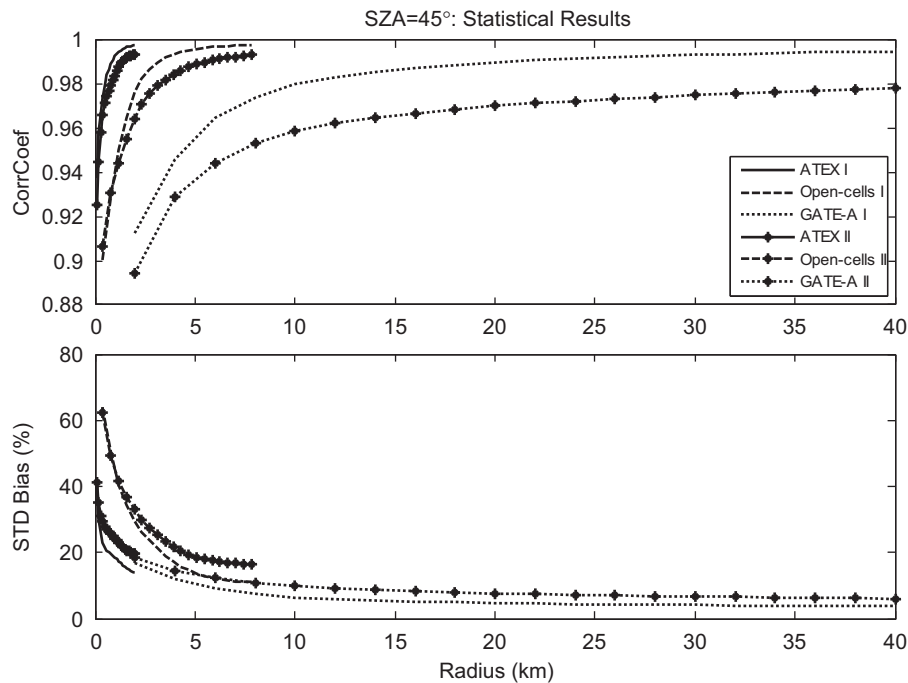

Fig. 9. The average *CorrCoef* and relative *STD_Bias* of three cloud fields calculated by both methods changing with statistic radius when SZA is 45°. Cloud fields are represented by different line types. The Lines without and with symbols mean the results of Methods I and II, respectively.

As shown in Fig. 9, different cloud fields have distinct characteristics of 3D effects on heating rate profiles. In particular, we compared Open-cells and GATE-A, since they have comparable range. The Open-cells cloud field mainly consists of high-level clouds with some optically thick low-level clouds, resulting in a quite high *CorrCoef*, for a given average radius. The scattered high-level clouds allow some photons reaching the lower portion of the atmosphere and heating the low-level clouds. Due to its inherently physical defects, the IPA cannot accurately reproduce the magnitude of low-level

heating, resulting in a large *STD_Bias*. The GATE-A cloud field is quite different from Open-cells, with more single-layer deep convective clouds. The 3D effects have greater impacts on the vertical distribution of heating rate with a smaller *CorrCoef* than on the heating rate strength with a better *STD_Bias*, with respect to the Open-cells. The ATEX with a better resolved cloud field has good *CorrCoef* and *STD_Bias*. Overall, it appears that the cloud 3D structures affect more in heating rate strength for ATEX and Open-cells, and more in vertical distribution for GATE-A.

Most previous studies used mainly the differences of strength between 3D and IPA to assess the 3D effects [34]. As we discussed above, the combination of *CorrCoef* and *STD_Bias* provides a better quantitative evaluation of the 3D effects. To better quantify the 3D effects, therefore, we set a threshold of *CorrCoef* at 0.99, and subsequently we seek its corresponding average radius and assess its associated *STD_Bias* in our three cloud fields. The *CorrCoef* threshold of 0.99 indicates that the IPA heating rate profiles are strongly correlated to the true 3D heating rate profiles. As listed in Table 1, for overhead sun, the critical radii of ATEX, Open-cells, and GATE-A are 0.16, 0.66, and 5.84 km, and the corresponding average *STD_Bias* values are 15.53%, 15.08%, and 5.08%, respectively. For the SZA of 60°, the critical radii are increased substantially to 0.83, 3.19, and 15.46 km, respectively. The ratios of critical radii at the two SZAs, 5.2, 4.8, and 2.6, respectively, depending on the averaged cloud top heights in the cloud fields, are larger than the slant path ratio (2) at the two SZAs. The *STD_Bias* values, on the other hand, are increased to 34.01%, 32.00%, and 6.72%, respectively. These results corroborate the previous finding that the degree of cloud 3D radiative transfer effects strongly depend on solar incident angle. It is worth noting that some columns are excluded in sample numbers, as the *CorrCoef* for these columns cannot reach 0.99 within an averaged radius of 20 columns. Also, the critical radii for clear-sky columns are larger than for cloudy columns, and the corresponding

STD_Bias values for clear-sky columns are smaller than for cloudy columns. It suggests that the clear-sky column heating rate profile is significantly affected by surrounding cloud structures, particularly at small spatial scales.

5. Summary and conclusions

In order to seek ways to detect the cloud 3D effects, we have to better understand and quantitatively assess the 3D effects on broadband heating rate profiles, from both modeling and observational perspectives. Beyond evaluating transmittance, reflectance, and absorption, we used two parameters, *CorrCoef* and *STD_Bias*, to quantitatively assess both vertical distribution and strength of heating rate profiles. Those heating rate profiles are calculated by the full 3D and IPA approaches in three cloud fields at different SZAs. Also, two statistical methods are applied to represent the modeling and observational characteristics at different average radii (or resolutions).

Our 3D results were first validated against the benchmark of the ICRCCM, and showed good agreement with the benchmark. Secondly, the domain averaged 3D effects on transmittance, reflectance, and absorption were assessed. It indicated that the IPA tends to be more transmissive (less reflective) at low SZAs, and less transmissive (more reflective) at larger SZAs than the

Table 1
The effective radius (when the *CorrCoef* reaches 0.99), relative *STD_Bias* and samples of three cloud fields calculated by both methods at 0° and 60° SZA.

	Method I			Method II		
	All	Cloudy	Clear sky	All	Cloudy	Clear sky
ATEX (784 Samples)						
0°						
Radius (km)	0.16	0.11	0.21	0.23	0.13	0.36
STD_Bias (%)	15.53	21.84	7.34	17.58	24.91	8.36
Samples	784	440	344	781	437	344
60°						
Radius (km)	0.83	0.54	1.20	0.88	0.59	1.32
STD_Bias (%)	34.01	44.56	20.07	39.46	50.34	23.13
Samples	784	440	344	618	372	246
Open-cells (3844 Samples)						
0°						
Radius (km)	0.66	0.56	1.43	0.88	0.75	1.91
STD_Bias (%)	15.08	16.07	6.56	15.41	16.39	8.85
Samples	3844	3404	440	3844	3404	440
60°						
Radius (km)	3.19	3.04	4.40	3.37	3.26	4.84
STD_Bias (%)	32.00	33.33	20.67	32.67	33.33	24.00
Samples	3812	3402	410	2768	2570	198
GATE-A (25,921 Samples)						
0°						
Radius (km)	5.84	3.86	7.47	10.03	5.31	14.14
STD_Bias (%)	5.08	8.20	2.34	6.25	9.77	3.52
Samples	25,902	11,695	14,207	23,772	11,074	12,698
60°						
Radius (km)	15.46	15.57	15.36	16.43	13.33	18.79
STD_Bias (%)	6.72	8.96	4.48	6.72	10.45	4.48
Samples	23,599	10,803	12,796	12,977	5616	7361

3D, and the IPA column absorption is always less than the 3D with the maximum bias at an intermediate SZA, regardless of the cloud fields. Those are consistent with previous findings, and can be explained by the lack of horizontal transport in the IPA.

The 3D effects on heating rate profiles are largely determined by cloud vertical structures. Low-level clouds and clear-sky pixels are affected the most, as the high clouds block the incident solar radiation for the shadowing-effect and/or reflect the incident solar radiation for the illuminating-effect. These processes are the primary reason for the heating rate shift, as well as for retrieval errors from satellite observations, particularly for high-resolution applications. Furthermore, as illustrated in both case and statistical analyses, the cloud 3D structures affect more in heating rate strength for the one set of cloud fields, such as ATEX and Open-cells, and more in vertical distribution for others, such as GATE-A. It is crucial to use the combination of *CorrCoef* and *STD_Bias* for better quantitative evaluation of the 3D effects.

From our quantitative statistical analysis, there is no simple way to define a critical resolution (or average radius), within which the IPA heating rate profiles closely represent the true 3D heating rate profiles. It is clear that the critical radius (or resolution) strongly depends on solar incident angle as well as cloud vertical distribution, such as the mean cloud top height. Also, the critical radii for clear-sky columns are larger than for cloudy columns, although the corresponding *STD_Bias* values for clear-sky columns are smaller than for cloudy columns. It suggests that the clear-sky column heating rate profile is significantly affected by surrounding cloud structures. Furthermore, the difference between Methods I (Circle average) and II (Line or a fixed view average) is increasing with the average radius. As many derived heating rate profiles from observations with fixed view sensors, such as BBHRP products from current ARM facilities, the cloud 3D effects due to the dimensionality difference between the 3D clouds and 2D clouds significantly impact on the heating rate profiles.

Our study is based on limited cloud fields and contains some assumptions in model setting. The issues raised in this study warrant more detailed studies, including wider spectral range [25,26,41]. The erroneous heating rate distribution due to the simplification of the RT calculation would certainly impact on cloud formation and dynamics. Hence, as the resolution of CRM and GCM models improves, the accuracy of the approximation algorithms such as the IPA should be reassessed, in terms of the cloud 3D effects on the heating rate profile and their impacts on cloud formation and atmospheric circulations. More importantly, observational capability is needed for detecting the 3D effects in addition to current imaging instrument or vertically resolved active sensors. As photon path lengths are controlled by spatial distributions of scattering and absorption, the information of photon path length distribution inferred from a high-resolution oxygen A-band spectrometer provides a measure of the 3D cloud effects [42–44]. Our follow-up study will focus on how to use the information of photon path length distribution to study the cloud 3D effects on heating rate profiles.

Reference

[1] Barker HW. Broadband irradiances and heating rates for cloudy atmospheres. In: Marshak A, Davis AB, editors. 3D radiative transfer in cloudy atmospheres. Berlin: Springer; 2005. p. 450–4.

[2] Min Q, Joseph E, Duan M. Retrievals of thin cloud optical depth from a multifilter rotating shadowband radiometer. J Geophys Res 2004;109:D02201.

[3] Stephens GL. Cloud feedbacks in the climate system: a critical review. J Clim 2005;18:237–73.

[4] Wang Y, Lü D, Huo J. Determination of the optical thickness and effective particle radius of clouds from transmitted solar radiation measurements. Prog. Nat. Sci. 2007;17(10):1119–207.

[5] Intergovernmental Panel on Climate Change (IPCC). Climate Change 2007: Synthesis Report. Contribution of Working Groups I, II and III to the Fourth Assessment Report of the Intergovernmental Panel on Climate Change. Geneva, Switzerland: IPCC; 2007 p. 104.

[6] Titov GA. Radiative horizontal transport and absorption in stratocumulus clouds. J Atmos Sci 1998;55:2549–60.

[7] O'Hirok W, Gautier C. A three-dimensional radiative transfer model to investigate the solar radiation within a cloudy atmosphere. Part I: spatial effects. J Atmos Sci 1998;55:2167–79.

[8] Gu Y, Liou KN. Radiation parameterization for 3d inhomogeneous cirrus clouds application to climate models. J Clim 2001;14:2443–57.

[9] Barker HW, Davies JA. Solar radiative fluxes for stochastic, scale-invariant broken cloud fields. J Atmos Sci 1992;49:1115–26.

[10] Barker HW, Morcrette JJ, Alexander GD. Broadband solar fluxes and heating rates for atmospheres with 3D broken clouds. Q J R Meteor Soc 1998;124:1245–71.

[11] Loeb NG, Davies R. Observational evidence of plane parallel model bias: apparent dependence of cloud optical depth on solar zenith angle. J Geophys Res 1996;101:1621–34.

[12] Loeb NG, Coakley Jr JA. Inference of marine stratus cloud optical depths from satellite measurements-does 1D theory apply?. J Clim 1998;11:215–33.

[13] Stephens GL, Gabriel PM, Tsay SC. Statistical radiative transport in one-dimensional media and its application to the terrestrial atmosphere. Transp Theory Stat Phys 1991;20:139–75.

[14] Cahalan RF, Ridgway W, Wiscombe WJ, Gollmer S, Harshvardhan. Independent pixel and Monte Carlo estimates of stratocumulus albedo. J Atmos Sci 1994;51:3776–90.

[15] Barker HW. A parameterization for computing grid-averaged solar fluxes for inhomogeneous marine boundary layer clouds. Part I: methodology and homogeneous biases. J Atmos Sci 1996;53:2289–303.

[16] Barker HW, Wielicki BA, Parker L. A parameterization for computing grid-averaged solar fluxes for inhomogeneous marine boundary layer clouds. Part II: validation using satellite data. J Atmos Sci 1996;53:2304–16.

[17] Marshak A, Davis A, Wiscombe WJ, Titov G. The verisimilitude of the independent pixel approximation used in cloud remote sensing. Remote Sensing Environ 1995;52:71–8.

[18] Davis A, Marshak A, Cahalan RF, Wiscombe WJ. The Landsat scale break in stratocumulus as a three-dimensional radiative transfer effect: implications for cloud remote sensing. J Atmos Sci 1997;54:241–60.

[19] von Savigny C, Davis AB, Funk O, Pfeilsticker K. Time-series of zenith radiance and sueface flux under cloudy skies: radiative smoothing, optical thickness retrievals and large-scale stationarity. Geophys Res Lett 2002;29(17):1825.

[20] Marshak A, Davis A, Cahalan RF, Wiscombe WJ. Nonlocal independent pixel approximation: direct and inverse problems. IEEE Trans Geosci Remote Sensing 1998;36:192–205.

[21] Várnai T, Davies R. Effects of cloud heterogeneities on shortwave radiation comparison of cloud-top variability and internal heterogeneity. J Atmos Sci 1999;56:4206–24.
[22] Hinkelman LM, Evans KF, Clothiaux EE, Ackerman TP, Stackhouse Jr PW. The effect of cumulus cloud field anisotropy on domain-averaged solar fluxes and atmospheric heating rates. J Atmos Sci 2007;64:3499–520.
[23] Barker HW, Stephens GL, Fu Q. The sensitivity of domain averaged solar fluxes to assumptions about cloud geometry. Q J R Meteor Soc 1999;125:2127–52.
[24] Chen T, Zhang Y, Rossow WB. Sensitivity of atmospheric radiative heating rate profiles to variations of cloud layer overlap. J Clim 2000;13:2941–59.
[25] Chen Y, Liou KN, Gu Y. An efficient diffusion approximation for 3D radiative transfer parameterization: application to cloudy atmospheres. J Quant Spectrosc Radiat Transfer 2005;92:189–200.
[26] Gu Y, Liou KN. Cirrus cloud horizontal and vertical inhomogeneity effects in a GCM. Meteorol Atmos Phys 2006;91:223–35.
[27] O'Hirok W, Gautier C. Absorption of shortwave radiation in a cloudy atmosphere: observed and theoretical estimates during the second Atmospheric Radiation Measurement Enhanced Shortwave Experiment (ARESE). J Geophys Res 2003;108(D14):4412.
[28] Vogelmann AM, Ramanathan V, Podgorny IA. Scale dependence of solar heating rates in convective cloud systems with implications to General Circulation Models. J Clim 2001;14:1738–52.
[29] Fu Q, Cribb MC, Barker HW, Krueger SK, Grossman A. Cloud geometry effects on atmospheric solar absorption. J Atmos Sci 2000;57:1156–68.
[30] Khairoutdinov MF, Randall DA. A cloud resolving model as a cloud parameterization in the NCAR Community Climate System Model: preliminary results. Geophys Res Lett 2001;28:3617–20.
[31] Davis AB, Marshak A. Solar radiation transport in the cloudy atmosphere: a 3D perspective on observations and climate impacts. Rep Prog Phys 2010;73:026801.
[32] Grabowski WW, Smolarkiewicz PK. CRCP: a cloud resolving convection parameterization for modeling the tropical convecting atmosphere. Physica D 1999;133:171–8.
[33] Randall D, Khairoutdinov M, Arakawa A, Grabowski W. Breaking the cloud parameterization deadlock. Bull Am Meteor Soc 2003;84:1547–64.
[34] O'Hirok W, Gautier C. The impact of model resolution on differences between independent column approximation and Monte Carlo estimates of shortwave surface irradiance and atmospheric heating rate. J Atmos Sci 2005;62:2939–51.
[35] Di Giuseppe F, Tompkins AM. Three-dimensional radiative transfer in tropical deep convective clouds. J Geophys Res 2003;108(D23):4741.
[36] Li S, Min Q. The diagnosis of multi-layer clouds using photon path length distributions. J Geophys Res 2010 under review.
[37] Barker HW, Stephens GL, Partain PT, Bergman JW, Bonnel B, Campana K, et al. Assessing 1D atmospheric solar radiative transfer models interpretation and handing of unresolved clouds. J Clim 2003;16:2676–99.
[38] Grabowski WW, Wu X, Moncrieff MW, Hall WD. Cloud-resolving modeling of cloud systems during phase III of GATE. Part II: effects of resolution and the third spatial dimension. J Atmos Sci 1998;55:3264–82.
[39] Anderson WD, Grubišić V, Smolarkiewicz PK. Performance of a massively parallel 3D non-hydrostatic atmospheric fluid model. In: Proceedings of the International Conference on Parallel and Distributed Processing Techniques and Applications, Las Vegas, NV, Computer Science Research, Education, and Applications Tech, 1997, p. 645–51.
[40] Fu Q, Liou KN. On the correlated K-distribution method for radiative transfer in nonhomogeneous atmospheres. J Atmos Sci 1992;49:2139–56.
[41] Chen Y, Liou KNA. Monte Carlo method for 3D thermal infrared radiative transfer. J Quant Spectrosc Radiat Transfer 2006;101:166–78.
[42] Min Q, Harrison L. Joint statistics of photon pathlength and cloud optical depth. Geophys Res Lett 1999;26:1425–8.
[43] Min Q, Clothiaux EE. Photon path length distributions inferred from rotating shadowband spectrometer measurements at the Atmospheric Radiation Measurements Program Southern Great Plains site. J Geophys Res 2003;108(D15):4465.
[44] Min Q, Harrison L, Kiedron P, Berndt J, Joseph E. A high-resolution oxygen A-band and water vapor band spectrometer. J Geophys Res 2004;109:D02202.